Inorg. Chem. **2002**, *41*, 249–258

XAFS Investigation of the Structure of Aqueous Thorium(IV) Species, Colloids, and Solid Thorium(IV) Oxide/Hydroxide

J. Rothe,* M. A. Denecke, V. Neck, R. Müller, and J. I. Kim

Forschungszentrum Karlsruhe, Institut für Nukleare Entsorgung, Postfach 3640, D-76021 Karlsruhe, Germany

Received June 1, 2001

X-ray absorption fine structure (XAFS) spectroscopy at the Th L3 edge is applied for the characterization of crystalline, anhydrous ThO_2(cr), microcrystalline $ThO_2 \cdot xH_2O$(s), amorphous $ThO_n(OH)_{4-2n} \cdot xH_2O$(am), aqueous Th(IV) solutions, and colloidal suspensions up to p_cH 3.7. The microcrystalline, possibly hydrated thorium dioxide, is formed at p_cH 1.5–2.5 by precipitation from suspensions of 16–23 nm thorium dioxide colloids. The solubility data determined for this solid is several orders of magnitude lower than the values for amorphous Th(IV) hydroxide or hydrous oxide. The EXAFS spectrum of the isolated microcrystalline particles shows that their structure is different from that of anhydrous crystalline ThO_2(cr) and amorphous $ThO_n(OH)_{4-2n} \cdot xH_2O$(am) precipitated at higher pH and dried at room temperature. The solubility measured for the amorphous Th(IV) precipitate is comparable to that previously reported for a solid prepared in a similar manner. In other solubility studies with amorphous Th(IV) hydroxide or hydrous oxide, considerably higher thorium concentrations are measured at p_cH 3.5–5. The aqueous speciation is made by EXAFS for solutions prepared by careful coulometric titration under comparable conditions (p_cH and thorium concentration). The spectra of these solutions demonstrate the presence of a large amount of Th(IV) polynuclear species or colloids of small size, having a highly asymmetric Th–O coordination. The EXAFS spectrum of these colloids is similar to that of the amorphous solid.

Introduction

Systematic XAFS (X-ray absorption fine structure) investigation of different Th(IV) oxide/hydroxide solids and Th(IV) solutions at varying pH values allows characterization/identification of the predominant species present. However, no systematic XAFS study of Th(IV) solutions, other than strongly acidic[1] or high in carbonate concentration,[2] have yet been published. The Th^{4+}(aq) ion can be found as the predominant aqueous species only at pH < 3. Potentiometric titration in the pH range of 2.5−4 with thorium concentrations of 10^{-4}−10^{-2} mol/L demonstrates the formation of polynuclear or colloidal species.[3−7] Different oligomeric species are proposed in the literature on the basis of iterative fitting of the titration data.

Solubility data reported for amorphous Th(IV) precipitates, called either amorphous hydroxides $Th(OH)_4$(am) or hydrous oxides $ThO_2 \cdot xH_2O$(am), show considerable discrepancies.[8−13] This may be due to the fact that the reported solubilities do not refer to a well-defined solid phase but to hydrated oxyhydroxide $ThO_n(OH)_{4-2n} \cdot xH_2O$(am) with $0 \leq n \leq 2$, depending on the preparation method, pretreatment, alteration, and temperature.[9−15] Furthermore, the presence of colloids can also explain the widely scattered Th(IV) concentrations measured in the various solubility studies.[16]

* To whom correspondence should be addressed. E-mail: rothe@ine.fzk.de.

(1) Moll, H.; Denecke, M. A.; Jalilehvand, F.; Sandström, M.; Grenthe, I. *Inorg. Chem.* **1999**, *38*, 1795−1799.
(2) Felmy, A. R.; Rai, D.; Sterner, S. R.; Mason, M. J.; Hess, N. J.; Conradson, S. D. *J. Solution Chem.* **1997**, *26* (3), 233−248.
(3) Baes, C. F., Jr.; Meyer, N. J.; Roberts, C. E. *Inorg. Chem.* **1965**, *4*, 518−527.
(4) Baes, C. F., Jr.; Mesmer, R. E. *The Hydrolysis of Cations*; Wiley-Interscience: New York, 1976.
(5) Brown, P. L.; Ellis, J.; Sylva, R. N. *J. Chem. Soc., Dalton Trans.* **1983**, 31−34.
(6) Grenthe, I.; Lagermann, B. *Acta Chem. Scand.* **1991**, *45*, 231−238.
(7) Ekberg., C.; Albinsson, Y.; Comarmond, M. J.; Brown, P. L. *J. Solution Chem.* **2000**, *29*, 63−86.
(8) Nabivanets, B. I.; Kudritskaya, L. N. *Ukr. Khim. Zh.* **1964**, *30*, 891−895.
(9) Moon, H. C. *Bull. Korean Chem. Soc.* **1989**, *10*, 270−272.
(10) Ryan, J. L.; Rai, D. *Inorg. Chem.* **1987**, *26*, 4140−4142.
(11) Felmy, A. R.; Rai, D.; Mason, M. J. *Radiochim. Acta* **1991**, *55*, 177−185.
(12) Rai, D.; Felmy, A. R.; Sterner, S. M.; Moore, D. A.; Mason, M. J.; Novak, C. F. *Radiochim. Acta* **1997**, *79*, 239−247.
(13) Rai, D.; Moore, D. A.; Oakes, C. S.; Yui, M. *Radiochim. Acta* **2000**, *88*, 297−306.

10.1021/ic010579h CCC: $22.00
Published on Web 01/04/2002

Recently, Bundschuh et al.[17] investigated the solubility and colloid formation of Th(IV) at pH 1.5−2.5. Coulometric pH titration was combined with laser induced breakdown detection (LIBD) to determine the initial colloid formation as a function of p_cH ($p_cH = -\log[H^+]$) in a series of 3×10^{-2}−9×10^{-5} M Th(IV) solutions in 0.5 M HCl/NaCl. Considering colloids as small solid particles, their formation indicates that the solubility is just exceeded during the titration. The solubility product of $\log K°_{sp} = -52.8 \pm 0.3$ evaluated by this method refers to the freshly formed small particles with a mean diameter in the range of 16−23 nm. According to the particle-size effect described by Schindler,[18] the solubility product of the colloidal particles is expected to be about 1.0−1.4 log units higher than that of the bulk solid. The value obtained is in good agreement with $\log K°_{sp}(ThO_2(cr)) = -54.2 \pm 1.3$ calculated from thermochemical data for crystalline ThO_2(cr).[19] Hence, the freshly formed colloidal thorium particles in this pH range are believed to have a crystalline thorium dioxide structure.[17]

This work is a continuation and an extension of the study by Bundschuh et al.[17] The solubility is determined for a microcrystalline $ThO_2 \cdot xH_2O$(s) precipitate formed in these colloidal suspensions. Solubility is also determined for an amorphous precipitate of Th(IV) hydroxide or hydrous oxide for comparison. Structural information from XAFS investigation is made for crystalline and amorphous solids, aqueous species, and colloidal suspensions formed at different pH. Both EXAFS (extended X-ray absorption fine structure) and XANES (X-ray absorption near-edge structure) results are presented.

Reports of XAFS studies on the formation of actinide oxide/hydroxide "eigen-colloids" and Th L-edge XAFS investigations are sparse. Conradson[20] describes an XAFS investigation of Pu(IV) oxyhydroxide colloids, reporting observation of multiple, distinct Pu−O bonds due to the presence of different Pu−O moieties. Östhols et al.[21] investigated the adsorption of Th(IV) on amorphous silica. They exclude the observation of any Th−Th interaction for their sorption samples loaded up to 230% surface coverage and for a reference thorium hydroxide sample due to the spread of Th−Th distances in the disordered materials. Giaquinta et al.[22] compared the speciation of U(VI) and Th(IV) sorbed onto bentonite clay under ambient and hydrothermal conditions. The authors state that, in nontempered clay samples, Th(IV) displays a first shell coordination expected for hydrated atoms and an additional oxygen shell at 3.66 Å. The second shell is tentatively ascribed to a Th(IV)−clay interaction. In contrast, Th(IV) in the tempered sample is described as a ThO_2-like polynuclear species. The FT spectrum of this sample exhibits an additional peak at 3.93 Å, best represented as a Th−Th interaction. In the EXAFS investigation of aqueous Th(IV) carbonato species at different carbonate concentrations by Felmy et al.,[2] the enhanced amplitude of the distal oxygen due to the focusing effect of the collinear carbon atom is used to determine the number of complexing CO_3^{2-} ligands. This methodology is similar to that used by Allen et al.[23] for Pu(IV) nitrato complexes. EXAFS analysis of the Th^{4+}(aq) ion in acidic solution (1.5 M $HClO_4$) obtained by Moll et al.[1] shows a hydration number of 9−11 with a Th−O bond distance of 2.45 Å. These results are in contrast to previous large-angle X-ray scattering reports,[24] which claim Th(IV) coordination by only 8 water molecules. The local atomic structure in polycrystalline ThO_2 (thorianite) and $ThSiO_4$ (thorite) was analyzed by Wu et al.,[25] with emphasis on the thermally induced structural change upon heating from room temperature to 1500 °C.

The remainder of this paper is organized as follows: The next section outlines the sample preparation and experimental procedure of XAFS data collection and analysis. This is followed by a summary of the solubility determination and the results from EXAFS and XANES measurements. These results are then discussed. The proceeding summary of the XAFS investigation of Pu(IV) colloids[20] and studies of the Th L3 edge[1,2,21,22,25,35] provides the background for discussion of our results. Finally, conclusions are presented in the last section.

Experimental Section

Sample Preparation and Solubility Measurements. $Th(NO_3)_4 \cdot 4.5H_2O$ (pa), NaCl (pa), and HCl (ultrapure) are purchased from Merck. For further purification, NaCl is recrystallized twice. The solutions are prepared with ultrapure water from a water purification apparatus (Milli-Q-academic, Millipore). The solubility is measured batchwise in 10−20 mL PFA or glass vials. Under the present experimental conditions no significant sorption effect is observed. The Th(IV) concentration is determined photometrically by the arsenazo method[26] and by ICP-AES analysis.

A combination pH electrode (type ROSS, Orion Co.) is used to determine the p_cH in 0.5 M NaCl solution. For this purpose it is calibrated against standard solutions x M HCl/$(0.5 - x)$ M NaCl, with x in the range 0.001−0.1.

The coulometric titration combined with colloid detection by LIBD is performed with the equipment described elsewhere.[17]

A summary of the samples investigated by XAFS spectroscopy is found in Table 1. The description of the sample preparation is grouped in solids and liquids as given below.

Th(IV) Solids. Sample A [Crystalline Thorium Dioxide, ThO_2(cr)]. Crystalline, anhydrous ThO_2 (99.99%) is obtained from Alfa

(14) Grenthe, I.; Fuger, J.; Konings, R. J. M.; Lemire, R. J.; Muller, A. B.; Nguyen-Trung, C.; Wanner, H. *Chemical Thermodynamics Vol. 1. Chemical Thermodynamics of Uranium*; Elsevier (OECD, NEA-TDB), North-Holland: Amsterdam, 1992.
(15) Greiling, H.-D.; Lieser, K. H. *Radiochim. Acta* **1984**, *35*, 79−89.
(16) Neck, V.; Kim, J. I. *Radiochim. Acta* **2001**, *89*, 1−16.
(17) Bundschuh, T.; Knopp, R.; Müller, R.; Kim, J. I.; Neck, V.; Fanghänel, Th. *Radiochim. Acta* **2000**, *88*, 625−629.
(18) Schindler, P. W. *Adv. Chem. Ser.* **1967**, *No. 67*, 196−221.
(19) Rai, D.; Swanson, J. L.; Ryan, J. L. *Radiochim. Acta* **1987**, *42*, 35−41.
(20) Conradson, S. D. *Appl. Spectrosc.* **1998**, *52* (7), 252−279.
(21) Östhols, E.; Manceau, A.; Farges, F.; Laurent, C. *J. Colloid Interface Sci.* **1997**, *194*, 10−21.
(22) Giaquinta, D. M.; Soderholm, L.; Yuchs, S. E.; Wasserman, S. R. *J. Alloys Compound.* **1997**, *249*, 142−145.
(23) Allen, P. G.; Veirs, D. K.; Conradson, S. D.; Smith, C. A.; Marsh, S. F. *Inorg. Chem.* **1996**, *35*, 2841−2845.
(24) Johansson, G.; Magini, M.; Ohtaki, H. *J. Solution Chem.* **1991**, *20* (8), 775−792.
(25) Wu, Z.; Farges, F. *Physica B* **1999**, *266*, 282−289.
(26) Östhols, E.; Bruno, J.; Grenthe, I. *Geochim. Cosmochim. Acta* **1994**, *58*, 613−623.

Table 1. Summary of Samples Examined in This Study

ID	sample description
A	ThO_2(cr)
B	microcrystalline $ThO_2 \cdot xH_2O$(s)
C	$Th(OH)_4$(am)/$ThO_n(OH)_{4-2n} \cdot xH_2O$(am)
D	5.5×10^{-2} M Th^{4+}(aq) in 1.5 M $HClO_4$
E	2.2×10^{-2} M $Th(NO_3)_4$ in 0.5 M NaCl, $p_cH = 1.38$
F	2.8×10^{-2} M $Th(NO_3)_4$ in 0.5 M NaCl, $p_cH = 1.66$
G	5.0×10^{-3} M $Th(NO_3)_4$ in 0.5 M NaCl, $p_cH = 3.02$
H	4.3×10^{-3} M $Th(NO_3)_4$ in 0.5 M NaCl, $p_cH = 3.50$
I	2.2×10^{-2} M $Th(NO_3)_4$ in 0.5 M NaCl, $p_cH = 3.67$
J	5.8×10^{-3} M $Th(NO_3)_4$ in 0.5 M NaCl, $p_cH = 3.62$ (filtered sample I)

Aesar and additionally heated at 750 °C for 8 h. The X-ray diffraction pattern shows the typical ThO_2(cr) reflections as sharp peaks.

Sample B [Microcrystalline Thorium Dioxide, $ThO_2 \cdot xH_2O$(s)]. In some of the colloidal suspensions obtained in the pH titration−LIBD experiment of Bundschuh et al.,[17] the formation of a small amount of precipitate (approximately 1 mg) is observed after 1−4 weeks. The amount of solid is not sufficient for characterization by classical X-ray diffraction. The equilibrium Th(IV) concentrations in these solutions are measured from oversaturation after 100 and 160 days. Because a solubility of more than 6 orders of magnitude lower than that for amorphous Th(IV) solids is observed, the data cannot refer to amorphous solid and must refer to crystalline thorium dioxide. However, even after agglomeration of 20 nm colloids and subsequent precipitation, the crystallite size is expected in the submicrometer range and should have a large, hydrated surface. Therefore, we designate these precipitates as microcrystalline $ThO_2 \cdot xH_2O$(s). To prepare the XAFS sample, the solid material is separated by ultrafiltration and collected on a cellulose triacetate membrane microfilter (Sartorius 20kD, Centrisart C-4, area 28 mm^2, pore size ≈ 1.8 nm). The filter with the wet solid is covered with a thin polyethlyene (PE) film-disk and stoppered with epoxy resin glue.

Sample C [Amorphous $ThO_2 \cdot xH_2O$(am) or $Th(OH)_4$(am)]. The amorphous precipitate of Th(IV) hydrous oxide or hydroxide is prepared under argon atmosphere by slow titration of a thorium nitrate solution with carbonate-free NaOH (Baker). The precipitate is washed with water and dried at room temperature for 1 week in a vacuum desiccator. The X-ray powder diffraction pattern of the precipitate does not show any characteristic peaks or broadened bands. Assuming the chemical composition as $ThO_2 \cdot xH_2O$(am), the water content of $x = 2.4$ is determined by gravimetric analysis after drying the sample overnight at 800 °C. In the solubility study with this solid from undersaturation, constant Th(IV) concentration is obtained after 80 days. The Th(IV) precipitate prepared in a similar manner by Dzimitrowicz et al.[27] was found to be X-ray amorphous but included small ThO_2(cr) crystallites (<3−8 nm), as shown by transmission electron microscopy. Such a precipitate has a nonunique composition and consists of hydrated oxyhydroxide, $ThO_n(OH)_{4-2n} \cdot xH_2O$(am). In contact with aqueous solution, the solubility is finally controlled by a surface layer of $Th(OH)_4$(am).[16]

The solid samples **A** and **C** are prepared as PE tablets for XAFS measurements. Enough solid sample to attain an edge jump across the Th L3 absorption edge of 1.2−1.3 is dispersed in PE by grinding and then pressed as tablets.

Aqueous Th(IV) Solution Samples. Sample D [Th^{4+}(aq) Species]. Sample **D** is 5.5×10^{-2} M Th^{4+}(aq) in $HClO_4$, prepared by dissolving amorphous Th(IV) hydroxide in 1.5 M $HClO_4$.

Samples E−I. Th(IV) solutions at different p_cH are prepared by dissolving $Th(NO_3)_4 \cdot 4.5H_2O$ in 0.5 M HCl/NaCl solution and adjusting p_cH by coulometric titration. Sample **E** also contains the Th^{4+}(aq) ion (2.2×10^{-2} M), as does sample **D**, but prepared without prior removal of nitrate, with adjustment of ionic strength (0.5 M NaCl), at p_cH 1.38. This p_cH is below the onset of hydrolysis. According to the calculated aqueous speciation and LIBD measurements,[16,17] sample **F** consists of both the Th^{4+}(aq) ion and a small amount of microcrystalline $ThO_2 \cdot xH_2O$(s) colloids.

Samples I and J. In sample **I** (2.2×10^{-2} M Th^{4+}(aq) at p_cH 3.67), polynuclear species and amorphous colloids ($Th_x(OH)_y^{4x-y}$(aq) + $Th(OH)_4$(am)) are present. The presence of colloids in sample **I** is confirmed by LIBD. Removal of these colloids by 1 kD filtration (Filtron, pore size ca. 1.2 nm) is not successful. LIBD shows that immediately after filtration colloids of >5 nm are regenerated. In the filtered sample **J** (5.8×10^{-3} M Th^{4+}(aq) at p_cH 3.62), the Th(IV) concentration decreased by a factor of 3.8.

Aqueous solutions are sealed in 4 mL PE vials having 13 mm diameter for XAFS measurements. None of the solutions contain visible precipitates.

XAFS Measurements. X-ray absorption spectra at the Th L3-edge (16.3 keV) are recorded in the range of 16.12−17.27 keV, using synchrotron radiation at the Hamburger Synchrotronstrahlungslabor, HASYLAB, A1-endstation (DESY). The DORIS III storage ring is operated at a positron energy of 4.44 GeV, at beam currents in the range of 150−80 mA. All samples, with the exception of **B**, **G**, and **H**, are measured in transmission mode at room temperature. Argon-filled ionization chambers are used at ambient pressure for the detection of primary and transmitted beam intensities. A third ionization chamber is used in all cases for simultaneous detection of the transmission signal of a Y foil (4 μm) as reference for calibration of the monochromator energy scale. This is calibrated to the Y 1s ionization energy of 17.038 keV, which is assigned to the first inflection point in the first derivative of the Y reference foil spectrum. The XAFS spectra of samples **G**, **H**, and **B** are recorded using a 5-pixel low-energy germanium solid-state detector (Canberra-Packard Ultra-LEGe) for energy-dispersive collection of Th $L\alpha_{1,2}$-fluorescence radiation (12.97 and 12.81 keV).

The X-ray monochromator is equipped with a channel-cut Si⟨111⟩ crystal ($2d = 6.271$ Å), with the exception of sample **D**, which is previously measured with a Si⟨311⟩ crystal pair.[1] The ratio of the first ionization chamber signal and the DORIS III ring current (I_0/I_{DORIS}) is held constant during each measurement, and harmonic reduction is achieved by detuning the parallel alignment of the monochromator to 50−70% of the maximum beam intensity using a MOSTAB driven piezo-actuator.

Spectra are recorded with a step width as follows: a 10 eV step width for the 16.12−16.18 keV range; a 5 eV step width for 16.18−16.29 keV; a 0.4 eV step width for 16.29−16.325 keV. For the EXAFS region, from 16.325 to 17.32 keV, the increment is chosen equidistant in *k*-space, with a 0.03 Å^{-1} step width. Up to seven scans are averaged to improve the signal-to-noise ratio of the measurements.

XAFS Data Analysis. EXAFS data analysis is based on standard least-squares fitting techniques[28] using the UWXAFS program package,[29] developed by Newville et al. from the University of

(27) Dzimitrowicz, D. J.; Wiseman, P. J.; Cherns, D. *J. Colloid Interface Sci.* **1985**, *103*, 170−177.

(28) Sayers, D. E.; Bunker, B. A. In *X-ray Absorption: Techniques of EXAFS, SEXAFS and XANES*; Koningsberger, D. C., Prins, R., Eds.; J. Wiley & Sons: New York, 1988; pp 211−253.

(29) Stern, E. A.; Newville, M.; Ravel, B.; Yacoby, Y.; Haskel, D. *Physica B* **1995**, *208*, *209*, 117−120.

Table 2. Data Range and Metric Parameters Extracted by Least-Squares Fitting Analysis of EXAFS Spectra[a]

ID	fit range (Å) ($R-\Delta$)	shell	R (Å)	N	σ^2 (Å^2)	ΔE (eV)	R-factor
A	1.47−4.66	O1	2.41 (2.42)	8.0	0.0054	2.3	0.0241
		Th	3.98 (3.96)	12[b]	0.0042	4.7	
		O2	4.63 (4.64)	24[b]	0.0064	6.4	
B	1.47−4.54	O1	2.44	11.0	0.0096	2.4	0.0259
		O2	3.69	2.2	0.0022	2.0	
		Th	4.2	1.0	0.0032	11.0	
C	1.47−4.42	O1	2.46	6.6	0.0106[c]	6.7	0.0029
		O2	3.13	4.4	0.0109	15.8	
		Th	3.96	1.5	0.0065	8.9	
D	1.47−2.58	O	2.45	12.7	0.0072	4.1	0.0135
E	1.47−2.70	O	2.45	12.4	0.0078	4.2	0.0117
F	1.47−2.70	O1	2.46	12.7	0.0081	4.2	0.0178
	[3.56]	O2	3.64	3.8	0.0063	3.6	
G	1.59−2.70	O	2.46	11.6	0.0074	3.9	0.0268
H	1.59−2.70	O	2.51	10.6	0.0121[c]	7.5	0.0167
I	1.47−4.05	O1	2.50	9.4	0.0140[c]	6.9	0.0072
		O2	3.09	1.2	0.0007	6.9	
		Th	3.99	0.7	0.0032	11.0	
J	1.59−2.58	O	2.51	10.5	0.0103[c]	7.5	0.0102

[a] Errors are discussed in the text. In the case of sample F, [3.56] refers to extension of fitting range when including the more distant feature marked by an arrow (left panel of Figure 3). $S_0^2 = 0.82$. Parentheses indicate theoretical values from XRD results.[40] [b] Fixed values. [c] With inharmonic correction.

Washington, Seattle, WA. The region to about 700 eV above the Th L3-edge ($k \sim 13.5$ Å^{-1}) is investigated. The atomic background function ($\mu_0(E)$) is optimized with respect to spurious contributions below 1 Å in the k^1-weighted Fourier transform of the data using the *autobk* utility. The ionization energy (E_0), the origin for calculation of the $\chi(k)$-function, is fixed at the maximum of the most intense absorption feature, the white line (WL) in the individual spectra. To extract metric parameters (neighboring atomic distances (R), mean square radial displacements or EXAFS Debye−Waller factors (σ^2), coordination numbers (N)) from the EXAFS, model backscattering amplitude and phase shift functions for single and double scattering paths are calculated using FEFF8[30,31] and optimized as implemented in the *feffit* code. Prior to analysis, the k^3-weighted EXAFS spectra are Fourier transformed over a k-space range of ≈2.7−13 Å^{-1}, using symmetric square windows with $\Delta k = 0.1$ Å^{-1} "Hanning sills". All fitting operations are performed in R-space over the individual radial distance ranges given in Table 2. Special care is taken to avoid overinterpretation of the data beyond the limits defined by the number of independent points.[32] The amplitude reduction factor (S_0^2)[33] is fixed at 0.82. This value reproduces the theoretical coordination number for the first oxygen neighbors (N_{O1}) of 8 in the ThO_2 fluorite structure (fit parameter: $N_{O1}S_0^2 = 6.5$).

The *feffit* code evaluates randomly distributed fit uncertainties as the amount by which a given parameter changes, when values for all other parameters remain fixed, while maintaining the sum of squares of the difference between data and model (χ^2) below a certain limit (as suggested by Teo[32]). This procedure yields first oxygen neighbor distance (R_{O1}) uncertainty values of $\Delta R_{O1} \leq 0.01$ Å and $\Delta N_{O1} \leq 1-1.5$ for samples **A**, **B**, and **D**−**G** and of $\Delta R_{O1} \leq 0.06$ Å and $\Delta N_{O1\leq}$ 1.4−2.7 for samples **C**, **I**, **H**, and **J**. Determination of parameters for the more distant thorium backscatterers yields $\Delta R_{Th} \leq 0.04$ Å and $\Delta N_{Th} \leq 1.2$ for samples **B**, **C**, and **I**. Uncertainties associated with double scattering paths are significantly higher, amounting to more than 2% for ΔR and 150% for ΔN for oxygen double scattering paths in the fit to sample **C** and **I** spectra. The overall goodness of the fit evaluated by *feffit* is given as the "R-factor" (listed in the last column in Table 2), which is χ^2 scaled by the magnitude of data.[34] $R = 0.02$ signifies that theory and data agree within 2%.

XANES spectra for samples **B**, **C**, **E**, and **I** are isolated from single XAFS scans following subtraction of the background absorption, approximated as a linear function, and normalization of the edge jump to unity at 16.425 keV.

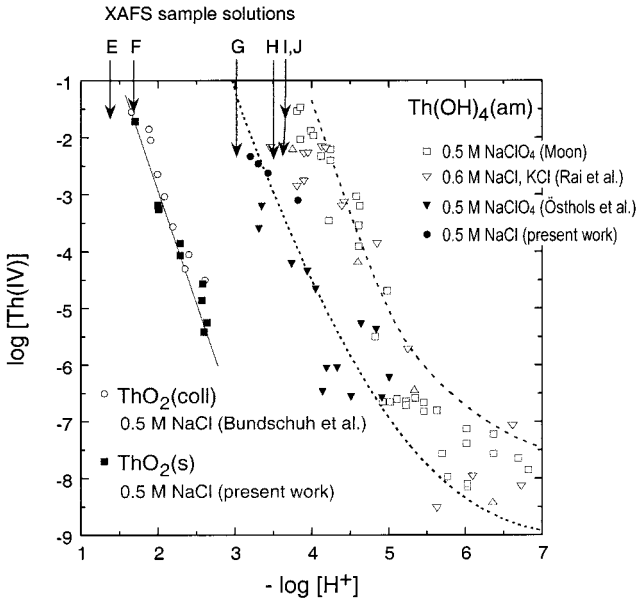

Figure 1. Solubility data for microcrystalline $ThO_2 \cdot xH_2O$(s) precipitates (present work) and colloids (LIBD study of Bundschuh et al.[17]) at 25 °C in 0.5 M NaCl and for amorphous Th(IV) precipitates (Moon,[9] Rai et al.,[11,12] Östhols et al.,[26] and present work) at $I = 0.5-0.6$ M and 18−25 °C. The calculated dashed curves for amorphous Th(IV) hydroxide represent upper and lower limits; the region between these curves represents the predominance region of polynuclear and colloidal Th(IV) species. Arrows indicate the H^+ and Th(IV) concentrations of the solutions investigated with XAFS, referring to sample ID's listed in Table 1.

Results

Solubility of Microcrystalline $ThO_2 \cdot xH_2O$(s) Particles. Th(IV) concentrations determined from oversaturation, 100 and 160 days after precipitation in the titration solution, are 0.4 log units lower (see Figure 1) than the data determined by Bundschuh et al.[17] for the 16−23 nm particles. This is consistent with the somewhat larger particle size, when colloidal particles agglomerate to form a visible precipitate. At $p_cH < 2.5$, where Th(IV) hydrolysis is negligible, the experimental solubility data for both colloidal and precipitated $ThO_2 \cdot xH_2O$(s) decreases with p_cH at a slope of −4. This indicates that the data actually refer to the equilibrium between $ThO_2 \cdot xH_2O$(s) and Th^{4+} (aq).

Our solubility measurements in Figure 1 are comparable with those obtained by Baes et al.[3] at 95 °C, who added crystalline ThO_2(cr) to oversaturated acidic Th(IV) solutions

(30) Ankudinov, A. L.; Ravel, B.; Rehr, J. J.; Conradson, S. D. *Phys. Rev. B* **1998**, *58*, 7565−7576.
(31) Ankudinov, A. L.; Rehr, J. J. *Phys. Rev. B* **1997**, *56*, 1712.
(32) Teo, B.-K. *EXAFS: Basic Principles and Data Analysis*; Springer-Verlag: Heidelberg, Germany, 1988.
(33) Lee, P. A.; Citrin, P. H.; Eisenberger, P.; Kincaid, B. M. *Rev. Mod. Phys.* **1981**, *53*, 769−806.
(34) Newville, M. *FEFFIT-Using FEFF to model XAFS data*; Department of Physics, FM-15, University of Washington: Seattle, WA, 1995.

in 1 M $NaClO_4$. Recently, Rai et al.[13] reported similar solubilities for ThO_2(cr) at 90 °C and pH 1.5−3 in 0.1 M NaCl. Under these conditions, an initially amorphous solid is converted into a crystalline phase. Their X-ray diffraction pattern showed broad bands at diffraction angles expected for bulk ThO_2(cr).

Solubility of Amorphous Th(IV) Precipitates. The solubility study with the amorphous Th(IV) precipitate is performed from undersaturation in 0.5 M NaCl solutions. The steady-state concentrations measured after an equilibration time of 80 days are shown in Figure 1 in comparison to literature data at similar ionic strength ($I = 0.5-0.6$ M). The present results are comparable with those of Östhols et al.[26] in 0.5 M $NaClO_4$ at 25 °C. These authors used a solid prepared in an analogous manner. The X-ray powder diffraction pattern of their precipitate indicated a low degree of crystallinity, and assuming the composition $ThO_2 \cdot xH_2O$-(am), the water content of their solid was determined[26] to be $x = 2.5$.

A number of other authors[8−13] performed their solubility study with amorphous precipitates, which were not dried but only washed with water. Their results are in reasonable agreement. However, they measured 3−4 orders of magnitude higher thorium concentrations in the p_cH range of 3.5−5 (cf. Figure 1). Those of Moon[9] and Rai et al.[11,12] at $I = 0.5-0.6$ M are typical examples. In both studies, the thorium concentration was determined after filtration through a pore size of about 2 nm to minimize contributions from colloids. The aim of our XAFS study is the aqueous speciation at thorium and H^+ concentrations comparable to those in the solubility studies (cf. Figure 1) to help elucidate the reason for the discrepancy between solubility data.

EXAFS Measurements. The k^3-weighted EXAFS functions, $\chi(k)$, extracted using *autobk* are shown in Figure 2 at left and the corresponding Fourier transform (FT) magnitudes at the right-hand side. All spectra exhibit an intense FT peak at 1.9 Å, corresponding to a phase-corrected value of about 2.4−2.5 Å. This peak represents oxygen atoms comprising the first coordination sphere of the central absorbing Th(IV) in all of the samples. A pronounced feature between about 1 and 1.5 Å, representing a low-frequency contribution to the EXAFS, is present in all spectra, even in spectra measured during different beam times and with different monochromator setups. This feature is apparently not an artifact of the μ_0 spline function subtraction, because it is persistent in the FT spectra, except for cases where the μ_0 subtraction is so extreme as to intolerably remove intensity of the Th−O peak at $R - \Delta = 1.9$ Å. Other Th L3 edge EXAFS presented in the literature also show a low-R feature in the FT spectra.[35] A Th−O distance of less than 2 Å makes no physical sense (the sum of ionic radii is 2.34 Å for 6-fold coordination[36]), so that we expect these features to be due to atomic contributions or to multielectron excitations in the EXAFS regime.[37] Supporting the latter hypothesis, the FEFF8

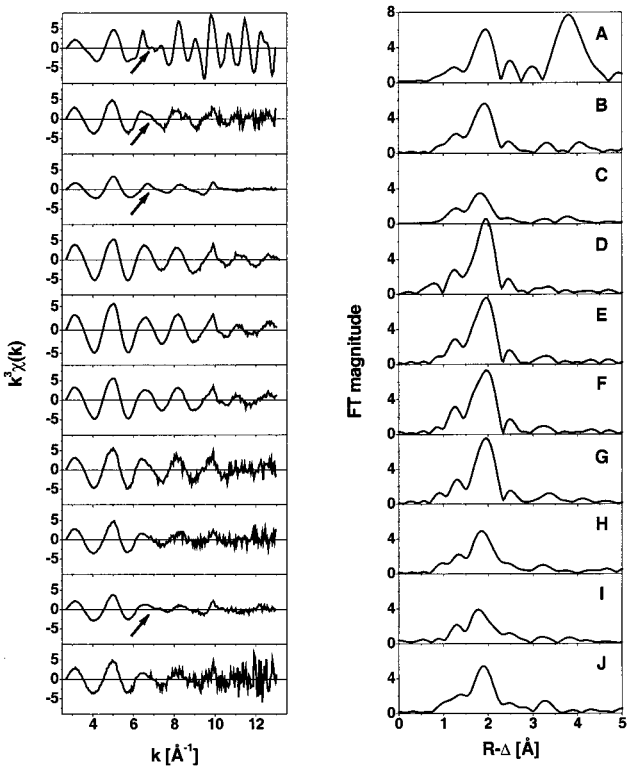

Figure 2. k^3-weighted $\chi(k)$ functions of the samples listed in Table 1, as extracted by *autobk* (left panel), and corresponding Fourier transform magnitudes (right panel). Arrows mark onset of high-frequency contribution due to Th−Th interaction.

calculation using a 45 atom cluster with cartesean coordinates from the ThO_2 fluorite structure yields a theoretical energy-dependency of μ_0 with discontinuities, evidence for multielectron excitations.[38] Despite its continual presence, inclusion or omission of this low-R feature by broadening or narrowing the R-space fit range does not significantly influence the metrical parameters obtained.

Fit results of the spectra to the EXAFS equation are summarized in Table 2. The metrical parameters obtained, principle component analysis (PCA), and visual inspection of the spectra allow grouping of the samples into three different sets. Figures 3, 4, and 6 show the fit results, grouped according to the three sample sets. The first group (aqueous solutions at $p_cH \leq 3$; samples **D**−**G**) exhibit spectra dominated by a single sinusoidal contribution originating from backscattering on a single shell of oxygen atoms. Uniqueness test of the solution spectra at $p_cH \leq 3$ with PCA[39] shows that they are similar. Sample **A**, the crystalline ThO_2 reference, as well as solid samples **B**, **C**, and the colloidal suspension **I** exhibit a more complex absorption fine structure and form the second group. The more complex fine structure includes the appearance of a high-frequency EXAFS contribution, indicated by arrows in the left panel of Figure 2, which is found in the fit procedure to be associated with a Th−Th interaction. Reproduction of the EXAFS for these

(35) Denecke, M. A.; Bublitz, D.; Kim, J. I.; Moll, H.; Farkes, I. *J. Synchrotron Radiat.* **1999**, *6*, 394−396.
(36) Greenwood, N. N.; Earnshaw, A. *Chemistry of the Elements*; VCH Verlagsgesell-schaft: Weinheim, Germany, 1988.
(37) Wang, W.-C.; Yu, C. *Phys. Status Solidi a* **1998**, *168*, 351−357.
(38) Rehr, J. J.; Zabinsky, S. I.; Ankudinov, A.; Albers, R. C. *Physica B* **1995**, *208*, *209*, 23−26.
(39) Wassermann, S. R.; Allen, P. G.; Shuh, D. K.; Bucher, J. J.; Edelstein, N. M. *J. Synchrotron Radiat.* **1999**, *6*, 284−286.

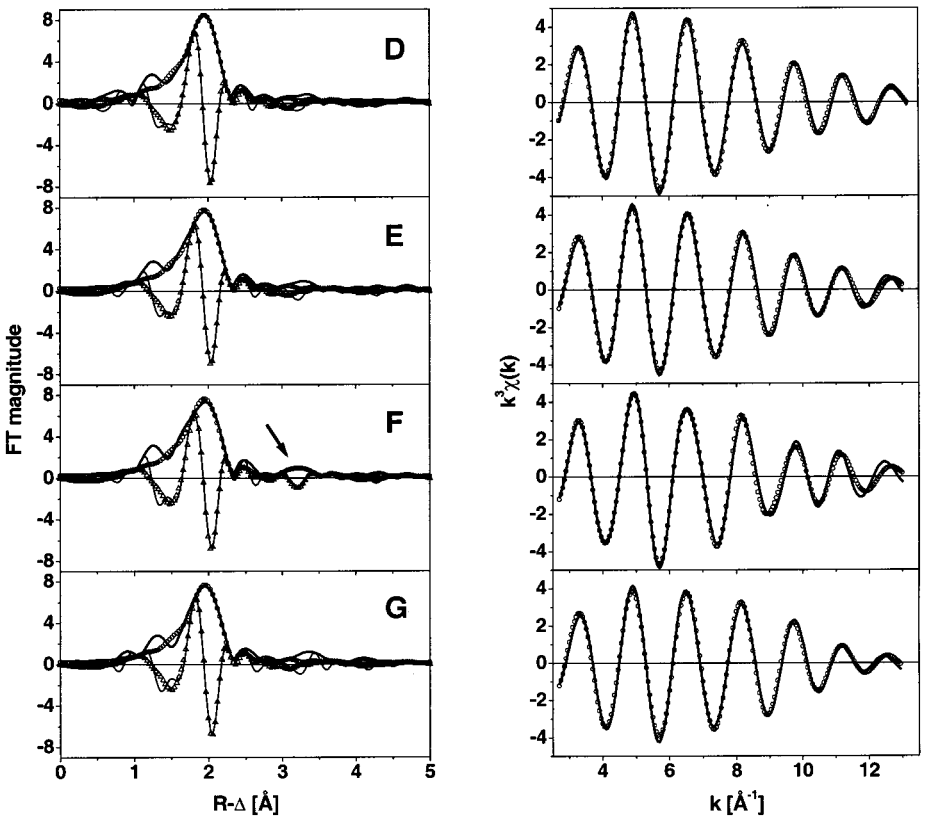

Figure 3. *R*-space fit results for solutions at $p_cH \leq 3$ (samples **D**−**G**). Left panel: FT magnitude of EXAFS data (solid line); fit magnitude (open circles); FT imaginary part (thin solid line) and fit imaginary part (open triangles). Right panel: corresponding Fourier-filtered data (solid line, ranges given in Table 2); back-transformed fit (open circles). The arrow in row **F** marks the feature due to a second oxygen distance at around 3.6 Å (see text).

four samples is only possible when the PCA-derived component with primarily a Th−Th oscillation is included. Spectra and fit results for samples **J** and **H** (aqueous solutions at p_cH 3.5 and 3.6) are similar and are placed into the third group. PCA uniqueness test of the spectra from these two aqueous solutions show that they are similar to one another and dissimilar to the spectra of solutions at $p_cH \leq 3$.The following discussion of the results is structured according to these three different groups of sample sets.

Samples D−G. The fits and experimental FT magnitudes for samples **D**−**G** and the corresponding Fourier-filtered data are shown in Figure 3. The small features at around 2.5 Å are attributed to artifacts of the FT procedure ("side-lobes"). The EXAFS spectra for these four solutions in the p_cH range 0−3 exhibit the signature of Th^{4+}(aq) species. They all have approximately the same metric parameters, 11.6−12.7 oxygen atoms at 2.45−2.46 Å, with $\sigma^2 = 0.007-0.008$ (Table 2). However, the fit to the oxygen peak in the *k* region above11 $Å^{-1}$ visibly worsens with increasing p_cH, going from sample **D** (in 1.5 M $HClO_4$) to **F** (p_cH 1.66, above the solubility limit for microcrystalline $ThO_2 \cdot xH_2O$(s)). This is due to the increasing asymmetry of the oxygen peak, evidenced by an increase in σ^2 from 0.0072 in sample **D** to 0.0081 in sample **F**. Sample **G** is a Th(IV) solution at the onset of hydrolysis ($p_cH = 3.02$). According to the hydrolysis constants discussed in ref 14, the following aqueous speciation is calculated: 59% Th^{4+}(aq); 31% $Th(OH)^{3+}$(aq); 1% $Th(OH)_2^{2+}$(aq); 8% dimeric and 1% tetrameric hydrolysis species. The EXAFS analysis of this sample's spectrum yields essentially the same metrical parameters as for samples **D**−**F**.

In addition to the low-*R* feature and the oxygen peak at 1.9 Å, the nitrate solution samples **E**−**G** exhibit a further distinct peak between 3 and 3.5 Å. This further distant peak is not obvious in the FT of Th^{4+}(aq) in 1.5 M $HClO_4$ (sample **D**). Three different multiple scattering paths can be envisaged to potentially be responsible for this peak: a double scattering, triangular path between Th(IV) and two adjacent oxygen atoms of the hydration/nitrate sphere, scattering on distal oxygen atoms of a bidentate coordinating nitrate, enhanced by the "focusing effect" of the collinear nitrogen atom of the nitrate ligand, and scattering on the nitrogen atom of a monodentate coordinating nitrate along the collinear Th−O−N path. Testing the triangular multiple scattering path shows that it entirely mismatches the experimental phase and magnitude of the ∼3.3 Å peak. We also rule out the second possibility by comparing results for aqueous Pu(IV) nitrate complexes reported by Allen et al.[23] Considering the larger ionic radius for Th(IV) compared to Pu(IV), one would expect a FT peak more distant ($R_{Th-O} \geq 4.15$ Å) than that actually observed. Due to a complete mismatch in phase and magnitude, scattering on a nitrogen atom of a monodentate coordinating nitrate group, enhanced by the bonding oxygen atom, can be excluded as well. Best fit results for sample **F**, when the fit range is extended to 3.56 Å, are obtained using a single scattering shell of about 4 oxygen atoms at 3.66 Å

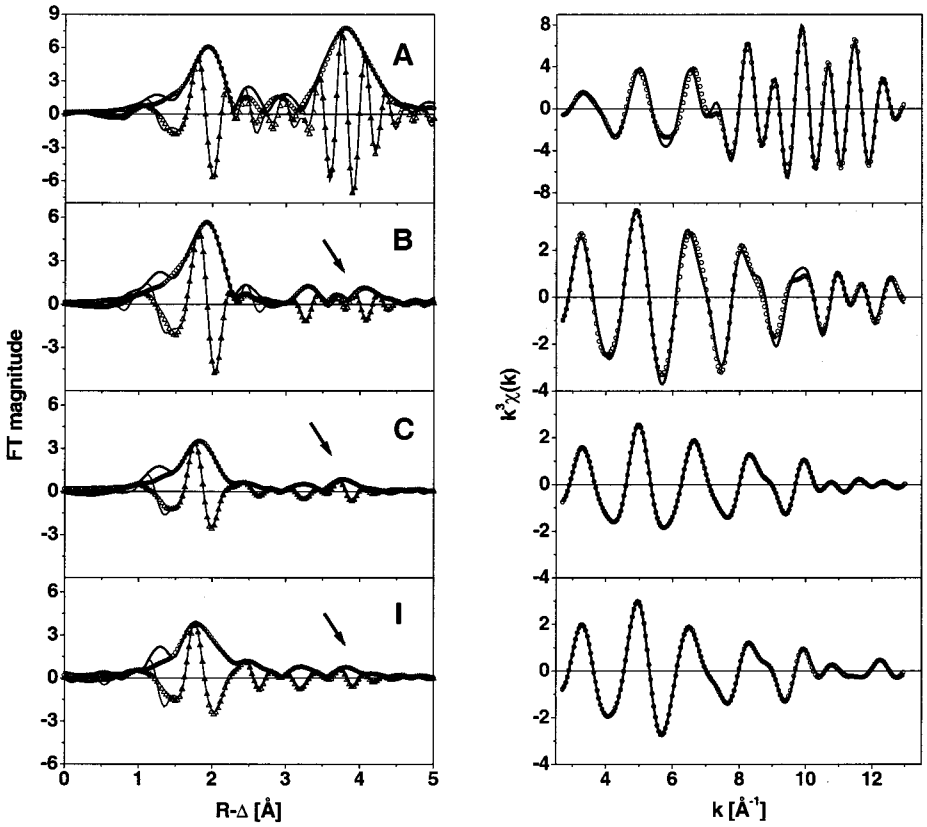

Figure 4. *R*-space fit results for solid samples (**A**−**C**) and aqueous colloidal suspensions (**I**). Left panel: FT magnitude of EXAFS data (solid line); fit magnitude (open circles); FT imaginary part (thin solid line) and fit imaginary part (open triangles). Right panel: corresponding Fourier-filtered data (solid line, ranges given in Table 2); back-transformed fit (open circles). Arrows mark Th−Th interaction in samples **C**, **I**, and **B**. Note the different ordinate scale for sample **A**.

(see arrow in left part of Figure 3). Fits performed in an analogous manner, using single scattering from an additional oxygen shell, yield unsatisfactory results for samples **E** and **G**.

Samples A−C and I. Results for solid samples **A**−**C** and the colloidal suspension **I** and the corresponding Fourier-filtered data are shown in Figure 4. The spectrum of the crystalline ThO_2 reference **A** has been modeled using single scattering paths of the first three shells of thorium neighbors (oxygen shell at 2.42 Å, thorium at 3.96 Å, and oxygen at 4.63 Å[40]). Theoretical values expected for the fluorite structure are reproduced within the typical margins of EXAFS uncertainties. There is a small fit mismatch in the region of the side lobes between 2.3 and 3.2 Å, reflected by the discrepancy in the area of the beat between the low-frequency oxygen and the high-frequency thorium signals at ≈5.5−7.5 $Å^{-1}$.

The spectra of the amorphous precipitate (sample **C**) and the aqueous suspension of amorphous colloids (sample **I**) exhibit very similar structures. Above the spurious low-*R* feature, the major oxygen FT peak appears dampened and asymmetrically broadened. Two additional peaks surmounting the noise level are observed in both spectra between 2.9 and 3.5 Å and 3.5−4 Å. We did not succeed in modeling the FT between 1.5 and 2.9 Å using a single shell of oxygen backscatterers, even when including an additional asymmetry term (3rd cumulant) to the fit. Addition of a second oxygen scattering path (O2) leads to a reasonable fit for sample **C** with 6−7 oxygen atoms at 2.46 Å (the same Th−O distance observed for the aquo species) and 4−5 further distant oxygen atoms at 3.13 Å. The agreement between measurement and fit is generally worse for the amorphous colloids (sample **I**). In this sample, the majority of oxygen atoms (9−10) is located at a distance of 2.50 Å, which is significantly longer than that observed for ThO_2(cr), the amorphous $ThO_n(OH)_{4-2n}{\cdot}xH_2O$(am) precipitate, and the Th^{4+}(aq) ion with its hydrate sphere. The second oxygen path in this case yields a smaller contribution of about 1 atom at 3.09 Å. The large asymmetry of the Th−O shell in sample **I** is reflected by a σ^2 value of 0.014 $Å^2$ for the short O-distance path, despite the addition of the 3rd cumulant term in the fit. ΔE_0 for the two adjacent oxygen shells is confined to the same value in the analysis of sample **I**. However, this procedure yields a negative *N* value for the O2 shell for sample **C**. Therefore, ΔE_0 is allowed to vary independently, yielding a large ΔE_0 value (15.8 eV) for the O2 shell.

There is good agreement between FT imaginary part and magnitude of the fit and the experimental features located between 3.5 and 4 Å (arrows) using a Th−Th interaction for both samples **C** and **I**. In sample **C**, 1−2 thorium atoms

(40) Magini, M.; Cabrini, A.; Scibona, G.; Johansson, G.; Sandström, M. *Acta Chem. Scand. A* **1976**, *30* (6), 437−447.

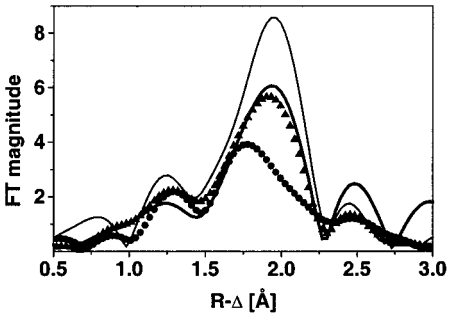

Figure 5. Comparison of the FT magnitudes of the Th^{4+}(aq) ion (sample **D**, thin solid line), crystalline ThO_2 (sample **A**, thick solid line), microcrystalline $ThO_2 \cdot xH_2O$(s) (sample **B**, black triangles), and the amorphous colloids (sample **I**, black dots).

at 3.96 Å are found; 1 thorium atom at 3.99 Å is observed in sample **I**.

The remaining peaks in the FT spectra of samples **C** and **I**, located between $R - \Delta = 3$ and 3.5 Å, are best fit using a triangular double scattering path between Th(IV) and two adjacent oxygen atoms: a Th → O_a → O_b → Th pathway, where the scattering amplitude is the greatest for near right angles between the two coordinating oxygen atoms (O_a and O_b) and the central thorium.

Sample **B** represents the microcrystalline $ThO_2 \cdot xH_2O$(s) particles initially formed in the acidic Th(IV) solution upon increasing p_cH (exceeding its solubility limit). Visual comparison of this sample's spectrum with those of crystalline, anhydrous ThO_2(cr) (**A**) and amorphous colloids (**I**) or $ThO_n(OH)_{4-2n} \cdot xH_2O$(am) precipitate (**C**) indicates that this sample's near-neighbor structure deviates significantly from both the crystalline and the amorphous structural conformations (Figures 2 and 4). The first Th−O neighbor coordination in sample **B** appears more ordered compared to the amorphous compounds but less ordered than the anhydrous ThO_2(cr) (sample **A**; cf. Figure 5). The fit for sample **B** yields $N = 11$, $R = 2.44$ Å, and $\sigma^2 = 0.0096$ Å^2, compared to $N = 8$, $R = 2.41$, and $\sigma^2 = 0.0054$ Å^2 for the bulk ThO_2-(cr). No second oxygen shell or inharmonic contribution is required to obtain a reasonable fit. The FT peak representing the Th−Th interaction in sample **B** (arrow in the right panel of Figure 4) is more pronounced than observed for the amorphous solids. However, the fit yields a Th−Th distance of 4.2 Å which is significantly increased compared to the bulk anhydrous ThO_2(cr) value of 3.96 Å.

Samples J and H. Samples **J** and **H** exhibit similar spectra (Figure 6). They have similar Th(IV) and H^+ concentrations but are prepared differently. Sample **J** is the 1 kD filtered sample **I**, and sample **H** is obtained by coulometric titration of a less Th(IV) concentrated solution. The EXAFS analysis yields almost identical metrical parameters for these samples (Table 2). These samples exhibit a strongly distorted first oxygen shell coordination, at an apparent Th−O bond distance of 2.51 Å. The fit converges by using a single oxygen shell. The spectra of both samples show no evidence for a Th−Th interaction near 4 Å. The features between $R - \Delta = 3$ and 3.5 Å are again best fit when using a single scattering oxygen path of about 3.6−3.9 Å, similar to sample **F**. However, the fit is not as exact in this case, so that any multiple scattering contribution (as in samples **C** and **I**) cannot be ruled out.

XANES Measurements. The XANES spectra for samples **B**, **C**, **E**, and **I** are depicted in Figure 7. A significant change in the intensity of XANES features is observed going across the series **E**, **B**, **I**, to **C**. The change is predominant for the WL. The WL intensity decreases going from the Th^{4+}(aq) ion (**E**) to the amorphous $ThO_n(OH)_{4-2n} \cdot xH_2O$(am) precipitate (**C**); the amorphous Th(IV) colloids (**I**) and microcrystalline $ThO_2 \cdot xH_2O$(s) (**B**) exhibit an WL intensity intermediate of these two.

Discussion

The metric parameters obtained for the solution samples **E** and **G** fully agree with results obtained in the previous EXAFS investigations of the Th^{4+}(aq) ion:[1] 10−12 water molecules (depending on the uncertainty in the S_0^2 value) coordinate Th(IV) at 2.45 ± 0.01 Å Th−O bond distance. There is no evidence for complexation by nitrate or chloride ligands under the present experimental conditions.

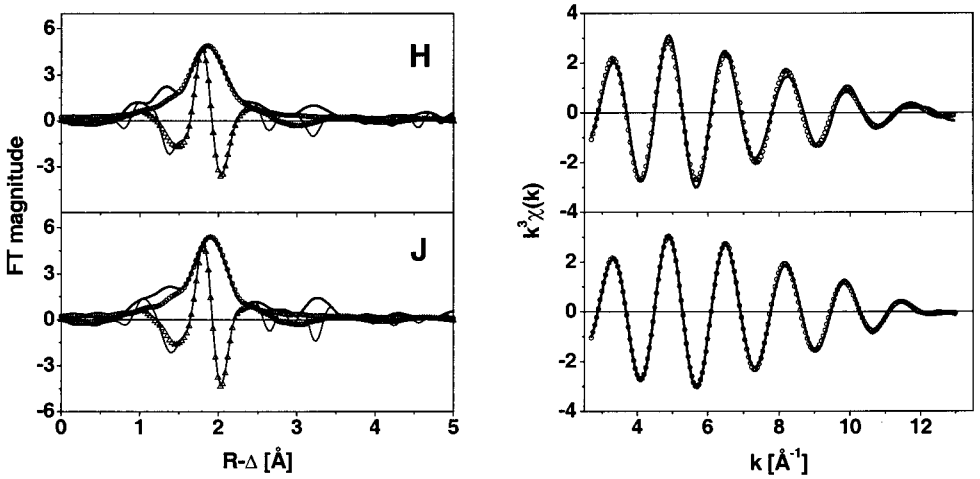

Figure 6. *R*-space fit results for aqueous samples **J** and **H** at p_cH 3.5 and 3.6. Left panel: FT magnitude of EXAFS data (solid line); fit magnitude (open circles); FT imaginary part (thin solid line) and fit imaginary part (open triangles). Right panel: corresponding Fourier filtered data (solid line, ranges as given in Table 2); back-transformed fit (open circles).

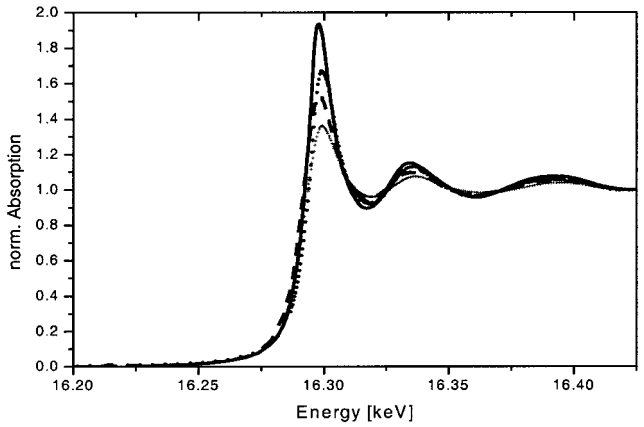

Figure 7. Th L3 edge XANES spectra for the Th^{4+}(aq) ion (solid line), microcrystalline $ThO_2 \cdot xH_2O$(s) (dotted line), the amorphous Th(IV) colloids (dashed line), and the amorphous $ThO_n(OH)_{4-2n} \cdot xH_2O$(am) precipitate (crosses).

Sample **F** is expected to exhibit a spectrum of the colloidal $ThO_2 \cdot xH_2O$(s) particles formed at the solubility threshold as detected by LIBD. However, most Th(IV) is apparently present in the form of aquo ions. However, the slight mismatch between the experimental XAFS oscillations of the first oxygen shell and theory in the *k*-range above 11 $Å^{-1}$ (see Figure 3) for this sample may indicate distortion of the Th(IV) hydrate sphere due to the presence of colloidal $ThO_2 \cdot xH_2O$(s) particles.

The agreement of experimental data and fit for the amorphous Th(IV) oxyhydroxide (sample **C**) and the suspension containing amorphous colloids at p_cH 3.67 (sample **I**) is satisfactory. A spread of Th−O distances is present in these samples, as reflected by their high-σ^2 values and the necessity to allow an additional inharmonic correction term for the O1 path. Furthermore, EXAFS for these two samples exhibits a particle size effect. The increased structural strain suffered by the smaller particles in the colloid sample **I** (larger surface-to-bulk ratio and, in turn, more surface dangling bonds) is seen in the greater asymmetric arrangement of its Th−O coordination sphere compared to sample **C**. Although the high asymmetry in these samples reflects the presence of different Th−O bond lengths from different coordinating oxygen atoms ($-O^-$, −OH, OH_2), the metric parameters obtained do not allow formulation of a precise structure model, as given by Conradson.[20] This is because the bond length resolution in EXAFS is limited by $\Delta R \approx \pi/2k_{max}$ (0.12 Å in this study), rendering it difficult, and for some distances impossible, to separate contributions from multiple, closely spaced backscatterers. Wu and Farges[25] describe the structural disorder in highly tempered ThO_2-(cr) by applying a model based on a probability distribution function rather than harmonic or cumulant expansion methods in the EXAFS analysis. The authors propose using such models for studying structurally complex Th-bearing oxides as well.

In contrast to the amorphous reference sample reported in the study by Östhols et al.,[21] the data for our amorphous $ThO_n(OH)_{4-2n} \cdot xH_2O$(am) and amorphous colloids unambiguously show the presence of Th(IV) backscatterers in EXAFS with Th−Th distances of 3.96 and 3.99 Å for samples **C** and **I**, respectively.

A comparison of the fluorescence XAFS spectra of sample **B**, microcrystalline $ThO_2 \cdot xH_2O$(s), and data presented in Figures 2 and 4 shows that the structure of sample **B** is different from that of the other samples studied. Its spectrum is definitely distinct from that of the amorphous species in **I** as well as the amorphous solid **C**. It is also different than the anhydrous ThO_2(cr). The Th−O FT peak for microcrystalline $ThO_2 \cdot xH_2O$(s), ThO_2(cr) , the amorphous solid, and amorphous colloids is compared in Figure 5. Visual inspection indicates that the oxygen next-neighbor coordination in sample **B** is most similar to ThO_2(cr). The near neighbor arrangement in these two samples, however, is not the same. The metrical parameters in the EXAFS analysis yield a higher N_{O1} value, a higher σ^2, and a longer Th−O bond distance for sample **B** compared to ThO_2(cr) (**A**). The "crystallinity" of this sample cannot be unambiguously deduced from the spectra and the metric parameters given in Table 2. The FT peak representing the Th−Th interaction (arrow in the left panel of Figure 4) is more pronounced than observed for the amorphous colloids. Whether the increased Th−Th distance of 4.2 Å is an artifact of the high asymmetry of the bonding or if it has to be assigned to the high degree of defect sites in the microcrystalline material, leading also to a strong reduction of the apparent Th−Th coordination number, is not yet clear.

The colloids and polynuclear species left in sample **J** after filtration of sample **I** still show the rather long Th−O first shell mean bond distance (2.51 Å) as observed for sample **I**. However, these colloids are apparently much smaller than those dominating the spectrum of sample **I**, as the spread of distances is reduced and the FT peak due to the Th−Th interaction is absent. These Th(IV) species seem to be similar to the "polynuclear" species in sample **H**; the two samples have nearly the same metric parameters and similar chemical composition.

There are two possible explanations for the WL intensity variations observed on the XANES regime. One is an extrinsic effect, resulting from charge transfer, and the other an intrinsic effect, resulting from the variation in crystallite size. The WL feature is associated with a dipole allowed transition from a $2p_{3/2}$ core level into an empty 6d state, lying just above the continuum or Fermi level (E_F). In the one-electron approximation, perturbation of the core hole on the d charge density is negligible.[41] Change in the intensity of the WL can result from variations in the occupancy of d states caused by a charge transfer between the central absorbing atom and its surrounding nearest neighbors, an extrinsic effect This is the basis of a method that has been used for estimating the amount of unoccupied d states from a relative change in WL areas (e.g., in refs 42 and 43). An example of an intrinsic, particle size effect leading to

(41) Benfatto, M.; Bianconi, A.; Davoli, I.; Incoccia, L. *Solid State Commun.* **1983**, *46*, 367.
(42) Mansour, A. N.; Cook, J. W.; Jr., Sayers, D. E. *J. Phys. Chem.* **1984**, *88*, 2330−2334.
(43) Lee, Y. S.; Whang, C. N.; Jeon, Y.; Choi, B. S.; Han, T. J.; Woo, J. J.; Croft, M. *Nucl. Instr. Methods Phys. Res. B* **1997**, *129*, 387−391.

variation in L3 XANES WL intensity has been reported for spectra of Pt nanoparticles.[44] WL intensity variation, in this case, results from variation of the averaged density of state (DOS) for atomic clusters as a function of the number of atoms in the cluster (or ratio of surface atoms to atoms in the bulk).

No significant variation in WL area, determined from least-squares fits to the data (not shown), is observed. From this we conclude that a transfer of charge from the surrounding coordinating atoms to Th(IV) is not responsible for the variation in the XANES WL intensity. If charge transfer is excluded, the WL intensity variation is likely a particle size effect and reflects variation in the DOS between the samples. Presently, the theoretical understanding of X-ray absorption WL's is not sophisticated enough to directly compare a DOS calculation with experimental spectra. However, qualitative trends can be made on the basis of experimentally observed trends in the WL intensity. Of the four Th(IV) sample spectra in Figure 7, the Th^{4+}(aq) ion has the most molecular orbital (MO)-like 6d final state. Because the $2p_{3/2} \rightarrow$ 6d dipole-allowed transition probability is proportional to the density of the 6d state, the MO-like, dense final state has the greatest transition probability of these samples and, hence, largest white line intensity. The 6d state of the condensed amorphous $ThO_n(OH)_{4-2n}{\cdot}xH_2O$(am) precipitate is no longer MO-like and better described as a band. The density of the 6d-like final state is lower for the band or electron cloud description, and the transition probability for the promotion of a $2p_{3/2}$ electron to this state decreases. With it, the intensity of the WL is observed to be lower than for sample **E**. The colloid and the microcrystalline samples represent an intermediate situation, and hence, their WL intensities are intermediate between the other two spectra. Small-sized Th particles make a qualitative rationalization of the 6d-like final state intermediary between the MO picture used for the aquo species and the band structure picture for the condensed, bulk system. In the small cluster, nonequivalent sites (surface sites and inner, core sites of the cluster) exist, making the average density of states near the Fermi level different from that of the MO picture. At the same time, the 6d-like final state is far from the bulk one in nanosized colloids. For large clusters, the average density should tend toward that of a band structure in the bulk system.

(44) Bazin, D.; Sayers, D.; Rehr, J. J.; Mottet, C. *J. Phys. Chem. B* **1997**, *101*, 5332−5336.

Conclusions

This paper describes the first XAFS investigation of the structure of Th(IV) oxide/hydroxide "eigen-colloids"—being the first ever to include XAFS measurements of actinide oxide/hydroxide colloids in the state of aqueous suspension. The application of XAFS spectroscopy for providing internal structural information of nanosized particles in situ is promising for further investigations in this area.

The solubility data reported recently for thorium colloids with a particle size of ~20 nm in the p_cH range of 1.5−2.5[17] and corresponding solid particles precipitated from these solutions refer to a microcrystalline thorium dioxide $ThO_2{\cdot}xH_2O$(s). They exhibit EXAFS spectra clearly different from amorphous $ThO_n(OH)_{4-2n}{\cdot}xH_2O$(am) and from that of bulk, anhydrous ThO_2(cr). Therefore, the structures of these microcrystalline particles must differ as well.

The EXAFS results for a solution consisting of both Th^{4+}(aq) ions and small amounts of microcrystalline $ThO_2{\cdot}xH_2O$(s) colloids (sample **F**) suggest distortion of the Th(IV) hydrate sphere due to formation of colloids above the solubility limit.

The high thorium concentration measured at p_cH 3.5−5 in numerous solubility studies with amorphous Th(IV) hydroxide or hydrous oxide presumably include a large amount of polynuclear species or amorphous Th(IV) colloids of ultrasmall size. This is concluded from the EXAFS spectrum for sample **I** solution at p_cH 3.67 in 0.5 M NaCl. In addition, the presence of colloids in this solution is confirmed by LIBD measurements. Polynuclear or colloidal species are also found immediately after ultrafiltration (sample **J**).

Acknowledgment. This work is partially supported by the European commission, in the frame of the ACTAF program within the fifth R&D framework program (Contract No. FIKW-CT-2000-00035). We gratefully acknowledge beam-time allotment from HASYLAB and experimental assistance from K. Attenkofer (HASYLAB), J.-M. Monsallier, and K. Dardenne (INE).

IC010579H